J|A|C|S
ARTICLES

Published on Web 06/30/2010

Flexibility of Shape-Persistent Molecular Building Blocks Composed of *p*-Phenylene and Ethynylene Units

Gunnar Jeschke,*[,†] Muhammad Sajid,[‡] Miriam Schulte,[‡] Navid Ramezanian,[‡] Aleksei Volkov,[§,¶] Herbert Zimmermann,[⊥] and Adelheid Godt*[,‡]

Laboratory for Physical Chemistry, ETH Zürich, 8093 Zürich, Switzerland, Department of Chemistry, Bielefeld University, Universitätsstrasse 25, D-33615 Bielefeld, Germany, Max Planck Institute for Polymer Research, Postfach 3148, 55021 Mainz, Germany, and Max Planck Institute for Medical Research, Jahnstrasse 29, 69120 Heidelberg, Germany

Received April 9, 2010; E-mail: godt@uni-bielefeld.de; gunnar.jeschke@phys.chem.ethz.ch

Abstract: Ethynylene and *p*-phenylene are frequently employed constitutional units in constructing the backbone of nanoscopic molecules with specific shape and mechanical or electronic function. How well these properties are defined depends on the flexibility of the backbone, which can be characterized via the end-to-end distance distribution. This distribution is accessible by pulse electron paramagnetic resonance (EPR) distance measurements between spin labels that are attached at the backbone. Four sets of oligomers with different sequences of *p*-phenylene and ethynylene units and different spin labels were prepared using polar tagging as a tool for simple isolation of the targeted compounds. By variation of backbone length, of the sequence of *p*-phenylene and ethynylene units, and of the spin labels a consistent coarse-grained model for backbone flexibility of oligo(*p*-phenyleneethynylene)s and oligo(*p*-phenylenebutadiynylene)s is obtained. The relation of this harmonic segmented chain model to the worm-like chain model for shape-persistent polymers and to atomistic molecular dynamics simulations is discussed. Oligo(*p*-phenylene butadiynylene)s are found to be more flexible than oligo(*p*-phenyleneethynylene)s, but only slightly so. The end-to-end distance distribution measured in a glassy state of the solvent at a temperature of 50 K is found to depend on the glass transition temperature of the solvent. In the range between 91 and 373 K this dependence is in quantitative agreement with expectations for flexibility due to harmonic bending. For the persistence lengths at 298 K our data predict values of (13.8 ± 1.5) nm for poly(*p*-phenyleneethynylene)s and of (11.8 ± 1.5) nm for poly(*p*-phenylenebutadiynylene)s.

Introduction

Poly(*p*-phenyleneethynylene)s (polyPPEs) and related compounds are shape-persistent polymers with applications in sensing and as organic conductors.[1−7] Due to their good synthetic accessibility oligomeric molecular building blocks of this type are a popular choice as parts of potential nanomachines,[8,9] for shape control of nanostructures in DNA-programmed self-assembly,[10] for constructing shape-persistent macrocycles,[11−13] and as active or passive spacers between electronically interacting moieties.[14−19] In such applications flexibility of the molecular backbone is an important issue,[20−23] but few experimental information appears to be available for this class of

† ETH Zürich.
‡ Bielefeld University.
§ Max Planck Institute for Polymer Research.
⊥ Max Planck Institute for Medical Research.
¶ Current address: BASF SE, 67063 Ludwigshafen, Germany.

(1) Weder, C., Ed. *Poly(arylene ethynylene)s: From Synthesis to Application*; Advances in Polymer Science, Vol. 177; Springer: Berlin, Heidelberg, New York, 2005.
(2) Bunz, U. H. F. *Chem. Rev.* **2000**, *100*, 1605–1644.
(3) Becker, K.; Lagoudakis, P. G.; Gaefke, G.; Höger, S.; Lupton, J. M. *Angew. Chem., Int. Ed.* **2007**, *46*, 3450–3455.
(4) Kim, I.-B.; Han, M. H.; Phillips, R. L.; Samanta, B.; Rotello, V. M.; Zhang, Z. J.; Bunz, U. H. F. *Chem.—Eur. J.* **2009**, *15*, 449–456.
(5) Thomas III, S. W.; Joly, G. D.; Swager, T. M. *Chem. Rev.* **2007**, *107*, 1339–1386.
(6) Kumaraswamy, S.; Bergstedt, T.; Shi, X.; Rininsland, F.; Kushon, S.; Xia, W.; Ley, K.; Achyuthan, K.; McBranch, D.; Whitten, D. *Proc. Natl. Acad. Sci. U.S.A.* **2004**, *101*, 7511–7515.
(7) James, D. K.; Tour, J. M. *Top. Curr. Chem.* **2005**, *257*, 33–62.
(8) Browne, W. R.; Feringa, B. L. *Nat. Nanotechnol.* **2006**, *1*, 25–35.
(9) Shirai, Y.; Osgood, A. J.; Zhao, Y.; Kelly, K. F.; Tour, J. M. *Nano Lett.* **2005**, *5*, 2330–2334.
(10) Gothelf, K. V.; Brown, R. S. *Chem.—Eur. J.* **2005**, *11*, 1062–1069.
(11) Höger, S. High-Yield Synthesis of Shape-Persistent Phenylene−Ethynylene Macrocycles. In *Functional Organic Materials: Synthesis, Strategies and Applications*; Müller, T. J. J., Bunz, U. H. F., Eds.; Wiley-VCH: Weinheim, 2007; pp 225−260.
(12) Weber, J.; Leppert, A.; Enkelmann, V.; Höger, S. *Beilstein J. Org. Chem.* **2008**, *4*, 1–15.
(13) Moore, J. S.; Zhang, J. *Angew. Chem., Int. Ed. Engl.* **1992**, *31*, 922–924.
(14) Lu, Q.; Liu, K.; Zhang, H.; Du, Z.; Wang, X.; Wang, F. *ACS Nano* **2009**, *3*, 3861–3868.
(15) Albinsson, B.; Mårtensson, J. *J. Photochem. Photobiol., C* **2008**, *9*, 138–155.
(16) Rochford, J.; Galoppini, E. *Langmuir* **2008**, *24*, 5366–5374.
(17) Azov, V. A.; Schlegel, A.; Diederich, F. *Angew. Chem., Int. Ed.* **2005**, *44*, 4635–4638.
(18) Guliyev, R.; Coskun, A.; Akkaya, E. U. *J. Am. Chem. Soc.* **2009**, *131*, 9007–9013.
(19) Weiss, E. A.; Ahrens, M. J.; Sinks, L. E.; Gusev, A. V.; Ratner, M. A.; Wasielewski, M. R. *J. Am. Chem. Soc.* **2004**, *126*, 5577–5584.
(20) Ballauff, M. *Angew. Chem., Int. Ed. Engl.* **1989**, *28*, 253–267.
(21) Bothner-By, A. A.; Dadok, J.; Johnson, T. E.; Lindsey, J. S. *J. Phys. Chem.* **1996**, *100*, 17551–17557.
(22) Göller, A.; Klemm, E.; Egbe, D. A. M. *Int. J. Quantum Chem.* **2001**, *84*, 86–98.

polymers. To the best of our knowledge no data have been published on temperature dependence of this flexibility and on the variation of flexibility with the sequence of ethynylene and phenylene repeating units. In designing molecular nanomechanical devices the type of bending potential and possible effects of thermal bending have to be considered.

The flexibility of shape-persistent oligomers and polymers can be elucidated from the end-to-end distance distribution.[24] Distances on the relevant length scale of a few nanometers can be measured between spin labels by pulse electron paramagnetic resonance (EPR) techniques[25−27] and distance distributions can be extracted from such data.[28−30] Recently we have demonstrated that by varying the length of the oligomer backbone, the contributions of the backbone and of spin labels attached to the chain ends can be separated.[31] This approach relies on coarse-grained modeling of the backbone by rigid segments linked by freely rotating joints with harmonic bending potentials. By refitting the backbone end-to-end distance distributions by the worm-like chain (WLC) model,[24,32,33] flexibility could be characterized by a single parameter, the persistence length L_p of the chain. Alternative EPR-based approaches for characterizing flexibility of oligoPPEs[34] and bis-peptides[35] were suggested at about the same time and the latter approach was recently extended to a coarse-grained model for bis-peptides.[36,37] The WLC model approach was recently applied to porphyrin-based molecular wires and a dependence of the mean end-to-end distance and width of the distance distribution on glass transition temperature of the solvent was found.[38]

Several important questions remained open in our first study. First, the quality of separation of the backbone and label contributions with the harmonic segmented chain (HSC) model was tested only *in silico* on data from a molecular dynamics (MD) simulation, but not experimentally. Indeed, when refitting the data for the individual backbone lengths of oligoPPE/Bs **I** (Chart 1) with the WLC model we found a trend in the persistence length whose origin and extent was not fully explained. Second, the backbones contained one butadiynylene unit, which may have a flexibility different from the one of ethynylene units. This structural imperfection may or may not have contributed to the trend in persistence length. Third, our measurements are performed at a cryogenic temperature of 50 K. As spontaneous chain bending is a consequence of thermal excitation, the persistence length needs to be specified together with a temperature.[38] To use our data for predictions of the behavior of nanomechanical devices on application of mechanical forces, the temperature corresponding to the measured end-to-end distance distribution and temperature dependence of the persistence length have to be known. This dependence is related to the shape of the bending potential.[39]

Chart 1. Structures of OligoPPE/Bs **I**, OligoPPEs **II**, OligoPPEs **III**, and OligoPPBs **IV**[a]

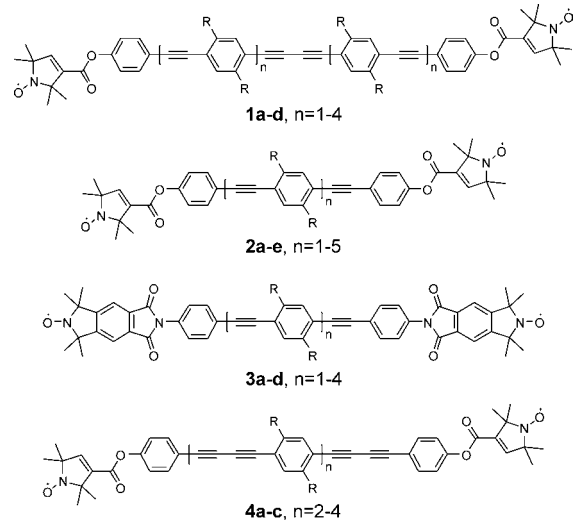

[a] Alk stands for hexyl as well as 6-methoxyhexyl substituents. For the sake of simplicity no differentiation between these two side chains is made here. The concrete structural formulae are given in Schemes 1−3.

In the present work, we address all these questions. In the Theoretical Calculations section we clarify the relation of the HSC model to the WLC model. Furthermore, we identify regimes where flexibility can or cannot be characterized by a persistence length. By synthesizing two series of oligo(*p*-phenyleneethynylene)s, oligoPPEs **II** and oligoPPEs **III** (Chart 1), with the same backbone structure but different spin labels, we are now able to verify experimentally the separation of the spin label from the backbone contribution. By comparing the series of oligo(*p*-phenylenebutadiynylene)s (oligoPPBs) **IV** to the series of oligoPPEs **II** with the same spin label, we can quantify differences between the flexibility of these two backbone types. By varying the glass transition temperature of the solvent over a wide range, we can test the hypothesis that the end-to-end distance distribution corresponds to the ensemble of chain structures frozen at the glass transition and the hypothesis that flexibility conforms to a harmonic bending potential. The paper concludes with considerations on further applications and tests of the HSC model.

Syntheses of Spin-Labeled OligoPPEs and OligoPPBs

Polar tagging is the common theme in the syntheses of the spin labeled oligomers, oligoPPEs **II** and **III** and oligoPPBs **IV**. The distinct influence of polar groups on the chromato-

(23) Allen, B. D.; Benniston, A. C.; Harriman, A.; Mallon, L. J.; Pariani, C. *Phys. Chem. Chem. Phys.* **2006**, *8*, 4112–4118.
(24) Wilhelm, J.; Frey, E. *Phys. Rev. Lett.* **1996**, *77*, 2581–2584.
(25) Milov, A. D.; Salikhov, K. M.; Shirov, M. D. *Fiz. Tverd. Tela (Leningrad)* **1981**, *23*, 975–982. *Sov. Phys. Solid State* **1981**, 565−569.
(26) Saxena, S.; Freed, J. H. *Chem. Phys. Lett.* **1996**, *251*, 102–110.
(27) Pannier, M.; Veit, S.; Godt, A.; Jeschke, G.; Spiess, H. W. *J. Magn. Reson.* **2000**, *142*, 331–340.
(28) Jeschke, G.; Koch, A.; Jonas, U.; Godt, A. *J. Magn. Reson.* **2002**, *155*, 72–82.
(29) Jeschke, G.; Panek, G.; Godt, A.; Bender, A.; Paulsen, H. *Appl. Magn. Reson.* **2004**, *26*, 223–244.
(30) Chiang, Y. W.; Borbat, P. P.; Freed, J. H. *J. Magn. Reson.* **2005**, *172*, 279–295.
(31) Godt, A.; Schulte, M.; Zimmermann, H.; Jeschke, G. *Angew. Chem., Int. Ed.* **2006**, *45*, 7560–7564.
(32) Kratky, O.; Porod, G. *Recl. Trav. Chim. Pays-Bas* **1949**, *68*, 1106–1122.
(33) Rubinstein, M.; Colby, R. H. *Polymer Physics*; Oxford University Press: Oxford, 2003.
(34) Margraf, D.; Bode, B. E.; Marko, A.; Schiemann, O.; Prisner, T. F. *Mol. Phys.* **2007**, *105*, 2153–2160.
(35) Pornsuwan, S.; Bird, G.; Schafmeister, C. E.; Saxena, S. *J. Am. Chem. Soc.* **2006**, *128*, 3876–3877.
(36) Pornsuwan, S.; Schafmeister, C. E.; Saxena, S. *J. Phys. Chem. C* **2008**, *112*, 1377–1384.
(37) Bird, G. H.; Pornsuwan, S.; Saxena, S.; Schafmeister, C. E. *ACS Nano* **2008**, *2*, 1857–1864.
(38) Lovett, J. E.; Hoffmann, M.; Cnossen, A.; Shutter, A. T. J.; Hogben, H. J.; Warren, J. E.; Pascu, S. I.; Kay, C. W. M.; Timmel, C. R.; Anderson, H. L. *J. Am. Chem. Soc.* **2009**, *131*, 13852–13859.
(39) Wilcoxon, J.; Schurr, J. M. *Biopolymers* **1983**, *22*, 2273–2321.

Scheme 1. Syntheses of Spin-Labeled OligoPPEs **3c**$_n$ and **5c**$_n$, alias OligoPPEs **II**, and Structural Formulae of Glaser Coupling Products **6**$_n$

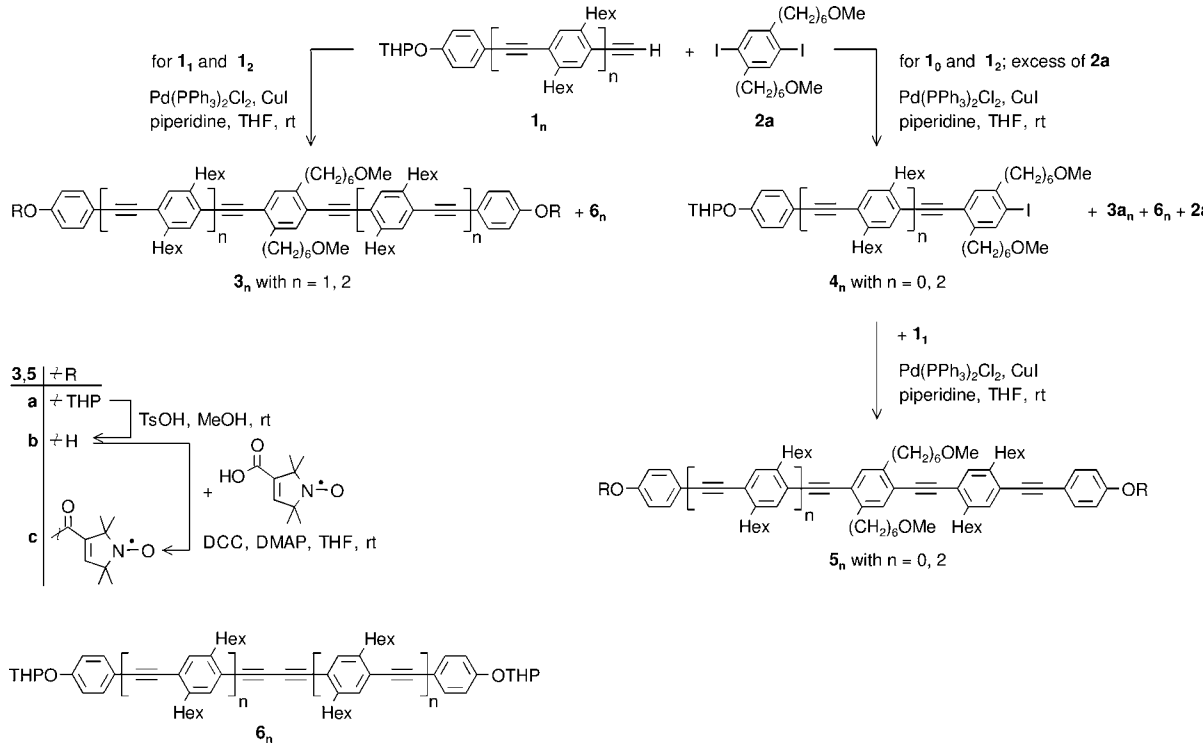

graphic behavior helped to isolate pure monodisperse oligomers and to keep the number of synthetic steps low. During the assembly of oligoPPEs **II** (Scheme 1) ether linkages in the side chains were used to make the alkynyl−aryl cross-coupling product very easily separable from the accompanying Glaser coupling (oxidative alkyne dimerization) product.[40] Ether linkages were also the key to obtain pure diiodotolane **2c** and were helpful in the isolation of oligoPPEs **III** (Scheme 2). The polar groups tetrahydropyran-2-yloxy (THPO), ether linkage, and hydroxymethyl were of great advantage for a straightforward access to the oligoPPBs **IV** (Scheme 3).

The symmetry of the oligoPPEs **II** and **III** with an uneven number of PPE units suggests to connect alkynes **1**$_n$ or **7**$_n$ via a 1,4-phenylene (Schemes 1 and 2). These alkynes are roughly half as long as the final oligoPPEs and bring along the required terminal functional groups, a protected OH group[41] or an isoindolineimide moiety. Deprotection of the hydroxyl group of the cross-coupling products obtained with alkyne **1**$_n$ followed by esterification with 1-oxyl-2,2,5,5-tetramethylpyrroline-3-carboxylic acid will give oligoPPEs **II**. Oxidation of the cross-coupling products from alkyne **7**$_n$ will yield oligoPPEs **III**. The pitfall of this approach is the Glaser coupling which is a regular companion of the alkynyl-aryl coupling.[42] Alkyne dimer will form from leftover alkyne upon exposure to air during workup. Traces of alkyne dimer may already be present before workup due to the use of a Pd(II) salt and the presence of oxygen in the reaction flask (despite careful degassing through freeze−pump−thaw cycles). The cross-coupling product and the Glaser coupling product differ only in one phenylene unit. On the basis of our finding that the polar end groups dominate the chromatographic behavior on silica gel and the number of 2,6-dihexyl-1,4-phenylene units displays only a marginal influence,[43] we expect the separation of the two products on a preparative scale to be insurmountable if nonpolar diiodobenzene **2b** is used as the connector. Therefore, we opted for polar tagging of the cross-coupling product with ether moieties in two of the side chains through the use of polar diiodobenzene **2a** as the connector.[40] Purposefully the ether moieties are separated from the phenylene moiety by a long alkyl spacer in order to avoid any electronic and/or steric influence on the backbone of the final oligomers. As expected, the Glaser coupling products **6**$_n$ were eluted well ahead of the cross-coupling products **3a**$_n$ from a silica gel column. This is demonstrated with the following R_f values (*n*-pentane/CH_2Cl_2 1/1): R_f(**3a$_1$**) = 0.14, R_f(**6$_1$**) = 0.83, R_f(**3a$_2$**) = 0.53, R_f(**6$_2$**) = 0.75. In the case of the bis(isoindolineimide)s **8a**$_n$ the ether moieties turned out to be insufficient for separating the cross-coupling products **8a**$_n$ from the Glaser coupling products **10a**$_n$ through standard column chromatography. To make the bis(isoindolineimide)s move on silica gel, ethanol had to be added to EtOAc or CH_2Cl_2 or $CHCl_3$. Under these elution conditions two more or less ether moieties seem to be insignificant if not detrimental, as is suggested by the finding that the cross-coupling products **8a**$_n$ are eluted shortly ahead of the Glaser coupling product **10a**$_n$ from a silica gel HPLC column ($CHCl_3$ with 5−10 vol % of MeOH). Neverthe-

(40) Sahoo, D.; Thiele, S.; Schulte, M.; Ramezanian, N.; Godt, A. *Beilstein J. Org. Chem.* **2010**, *6*; DOI: 10.3762/bjoc.6.57.

(41) The phenolic group does not interfere with the alkynyl−aryl cross-coupling, i.e. the tetrahydropyran-2-yl group is not necessary as a protection group. It is used because it eases the isolation of the products via chromatography.

(42) Carbometalation product is another byproduct which occured occasionally and only in traces. Its chromatographic behavior is similar to that of the corresponding Glaser coupling product. For further information see the Supporting Information.

(43) The oligomer that has the same structure as **5a$_0$** [however, with hexyl instead of methoxyhexyl as the side chains (R_f = 0.73)] and the dimer **6$_2$** [(R_f = 0.79)] differ in two PPE units. The oligomer that has the same structure as **5a$_1$** [however, with hexyl instead of methoxyhexyl as the side chains (R_f = 0.63)] and the dimer **6$_3$** [(R_f = 0.73)] differ in three PPE units. Despite these structural differences, the R_f values (silica gel; *n*-pentane/CH_2Cl_2, 1:1) are very similar.

Scheme 2. Syntheses of Bis(*N*-oxylisoindolineimide)s **8b$_n$** and **9b$_n$**, alias OligoPPEs **III**, and Structural Formulae of Glaser Coupling Products **10$_n$**

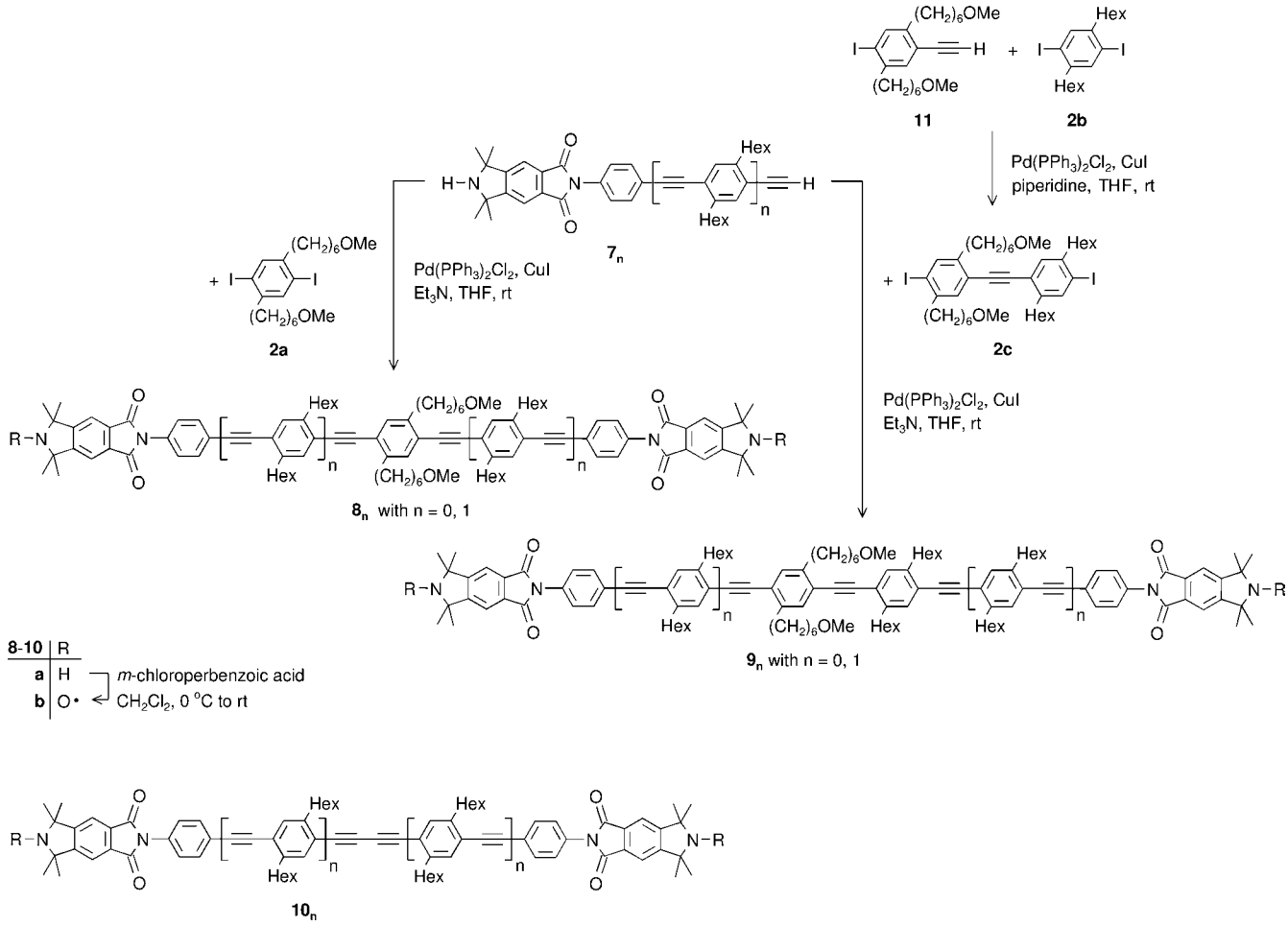

less, the isolation of bis(isoindolineimide) **8a$_1$** through HPLC was successful. The isolation of bis(isoindolineimide) **8a$_0$** via HPLC was not pursued. Instead, the mixture of bis(isoindolineimide)s **8a$_0$** and **10a$_0$** was treated with *m*-chloroperbenzoic acid and bis(*N*-oxylisoindolineimide) **8b$_0$** was isolated by standard column chromatography.[44]

Polar tagging with the ether moiety in the side chain was also valuable in the syntheses of oligoPPEs **II** and **III** with an even number of PPE units, i.e. of **5c$_n$** and **9b$_n$**. The precursors **5a$_n$** of the oligoPPEs **5c$_n$** were assembled in two steps (Scheme 1). First, alkynes **1$_n$** were coupled with polar diiodobenzene **2a** which was used in a 3-fold amount to minimize dicoupling. Second, the products **4$_n$** were coupled with alkyne **1$_1$** to obtain the oligoPPEs **5a$_n$**. The bis(isoindolineimide)s **9a$_n$**, the precursors of the spin labeled oligomers **9b$_n$**, were synthesized in the same manner as the bis(isoindolineimide)s **8a$_n$**, however with exchanging the connector diiodobenzene **2a** for diiodotolane **2c** (Scheme 2). In the preparation of the latter the ether moieties played a key role: Reaction of alkyne **11** with an excess of diiodobenzene **2b** gives a mixture mainly consisting of diiodotolane **2c** and residual diiodobenzene **2b**. Minor components are the Glaser coupling product and oligomers with three and more PPE units. All of these byproducts have more ether moieties than the target compound **2c** and thus are chromatographically easily removable. As had been found for the bis(isoindolineimide)s, **8a$_n$**, the isolation of the bis(isoindolineimide)s, **9a$_n$**, through standard column chromatography was unsuccessful despite polar tagging. Therefore, HPLC was employed to isolate the compounds before they were transformed into the bis(N-oxylisoindolineimide)s **9b$_n$** through oxidation with *m*-chloroperbenzoic acid. The alternative procedure, standard column chromatographical separation of the species at the stage of the bis(*N*-oxylisoindolineimide)s **9b$_n$** and **10b$_n$**, which are much less sticky toward silica gel than the precursors **9a$_n$** and **10a$_n$**, was successfully tested on bis(*N*-oxylisoindolineimide)s **9b$_1$** and **10b$_1$** [R_f(**9b$_1$**) = 0.59; R_f(**10b$_1$**) = 0.78; silica gel, CH_2Cl_2/Et_2O 9/1]. As can be seen from the given R_f-values, reducing the strong adhesion of the terminal functionalities through conversion of the amines into N-oxylamines makes the ether moieties in the side chains act again as the factor that dominates the rate of elution.

The syntheses of oligoPPBs **IV** (Scheme 3) resembles that of the oligoPPEs **II**: first, construction of the backbone with two terminal THPO groups, then removal of the THP moiety and attachment of the spin label through esterification with spin label 1-oxyl-2,2,5,5-tetramethylpyrroline-3-carboxylic acid.

For the syntheses of the backbones of the spin-labeled oligoPPBs **IV**, we decided in favor of the Glaser coupling, even when aiming for unsymmetrically substituted butadiynes. Glaser coupling of two different alkynes offers a rapid access to such butadiynes albeit at the expense of yield because half of the

(44) Sajid, M.; Jeschke, G.; Wiebcke, M.; Godt, A. *Chem.—Eur. J.* **2009**, *15*, 12960–12962.

Scheme 3. Syntheses of Spin-Labeled OligoPPBs **16c$_2$**, **21c**, and **16c$_4$**, alias OligoPPBs **IVa**−**c**

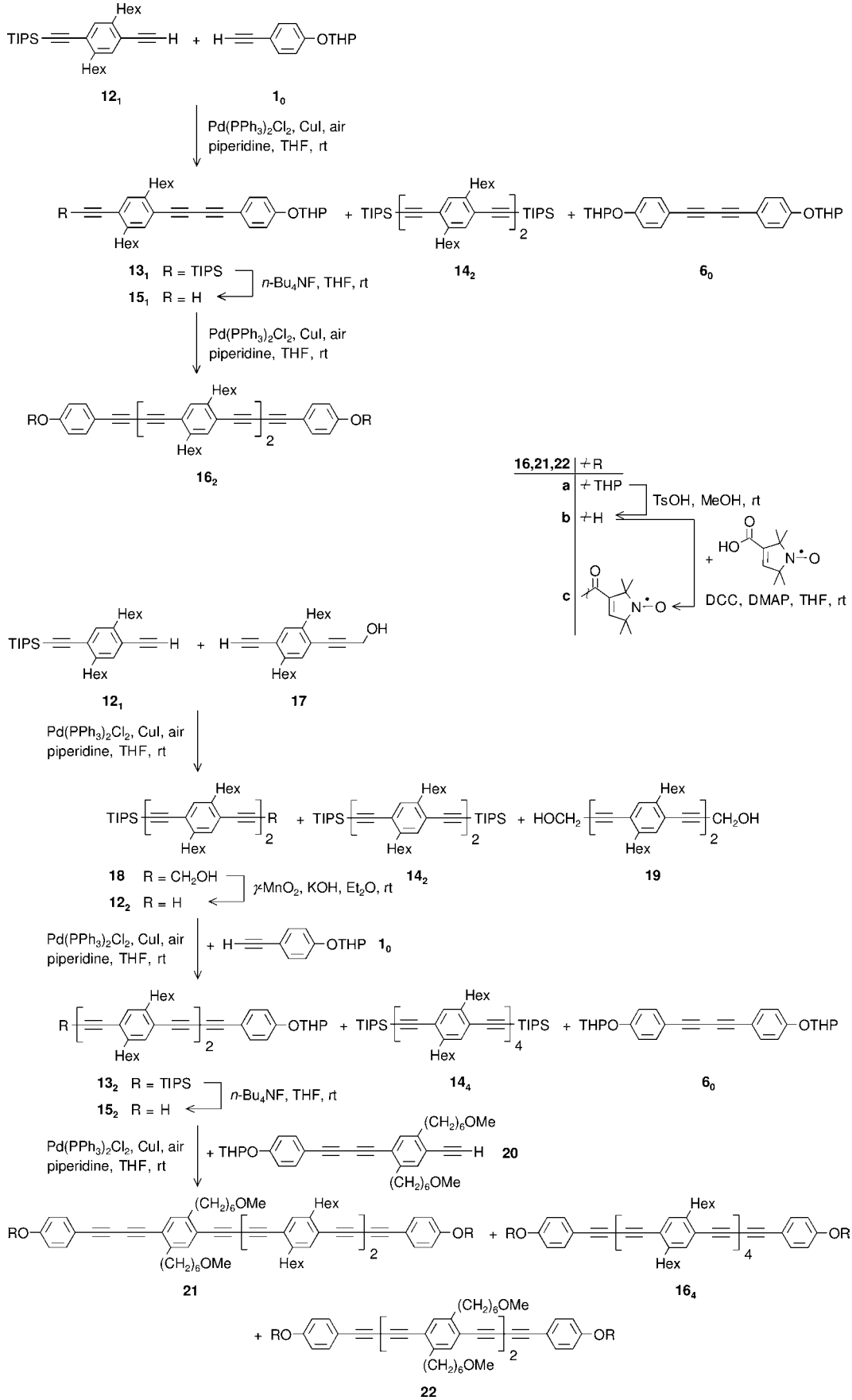

amount of the alkynes is consumed by the dimerization of identical alkynes (homodimerization). The Cadiot−Chodkiewicz coupling[45,46] may have been less material wasting. However, it would have required more synthetic steps because 1-bromoalkynes are involved. Furthermore, homodimerization is often a severe side reaction diminishing the advantage of the Cadiot−Chodkiewicz coupling over that of a random Glaser coupling. Whereas by accepting the low yields of a Glaser coupling with two different alkynes, no compromise was made in terms of time and effort needed for the isolation of the targeted compounds. By employing polar tagging, a simple standard column chromatography was sufficient to separate the three dimers−two homodimers and one heterodimer. The Glaser coupling was achieved with a mixture of $Pd(PPh_3)_2Cl_2$ and CuI in THF and piperidine in air.[47] Under these conditions the Glaser coupling is fast and, except when alkyne **17** is involved (Scheme 3), no byproducts were detected. Therefore, we decided to stay with this protocol.

The synthesis of spin-labeled oligoPPB $\mathbf{16c_2}$ starts with a Glaser coupling of the alkynes $\mathbf{12_1}$ and $\mathbf{1_0}$ (Scheme 3). The three products $\mathbf{13_1}$, $\mathbf{14_2}$, and $\mathbf{6_0}$ were easily separable because they differ in the number of the THPO groups and show very different times for elution from a silica gel column.[41] Through desilylation of heterodimer $\mathbf{13_1}$ and subsequent Glaser coupling the backbone construction was finalized.

Both spin-labeled oligoPPBs **21c** and $\mathbf{16c_4}$ originate from the nonpolar alkyne $\mathbf{12_1}$ and the polar alkyne **17**. Glaser coupling of these two alkynes was troublesome. It proceeded slowly and gave byproducts of unidentified structure. Nevertheless, heterodimer **18** was isolated as a pure compound. Removal of the polar hydroxymethyl group and Glaser coupling of the resulting nonpolar alkyne $\mathbf{12_2}$ with alkyne $\mathbf{1_0}$ gave a mixture of dimers from which the individual dimers were effortlessly isolated due to their distinctly different solubility and chromatographic behavior. The heterodimer $\mathbf{13_2}$ was desilylated, and the product, alkyne $\mathbf{15_2}$, was oxidatively coupled with alkyne **20** to complete the backbone assembly. With alkyne **20** ether moieties were introduced to simply pick the three individual products $\mathbf{16a_4}$, **21a**, and **22a** according to their number of polar side chains as demonstrated by the R_f values (silica gel, CH_2Cl_2): $R_f(\mathbf{16a_4}) = 0.83$, $R_f(\mathbf{21a}) = 0.45$, $R_f(\mathbf{22a}) = 0.05$. Alkyne **20** was synthesized following the protocol developed for the preparation of alkyne $\mathbf{15_1}$ (see Supporting Information).

Theoretical Calculations

Both the WLC and the HSC model are modifications of the freely rotating chain model. In the freely rotating chain model the polymer chain consists of n rigid segments with lengths l ($l_j = l$ for all j) linked by joints with fixed intersegment angle θ ($\theta_j = \theta$ for all j in all chains in an ensemble) and a torsion angle ϕ that is uniformly distributed between 0 and 2π corresponding to free rotation at the joints (Figure 1). The WLC model, which is a simplification of a more general model for linear chains by Kratky and Porod,[32,48] assumes a fixed angle

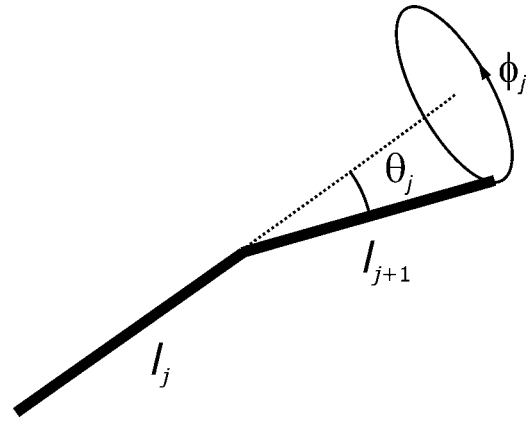

Figure 1. Parameters of segmented chain models. The chain consists of n segments with lengths l_j ($j = 1...\ n$) and intersegment angles θ_j ($j = 1...\ n-1$). In freely rotating chain models the torsion angles ϕ_j are equally distributed between 0 and 2π.

$\theta \ll 1$. The local correlations between segment vectors then decay on the scale of the persistence length L_p,

$$Lp = 2l/\theta^2 \tag{1}$$

By letting $l \rightarrow 0$ and $\theta \rightarrow 0$ at constant persistence length, the WLC model describes an unsegmented chain that can bend continuously and has a contour length $c_l = nl$. The mean square end-to-end distance $\langle R^2 \rangle$ of such a chain is given by

$$\langle R^2 \rangle = 2c_l L_p[1 - (L_p/c_l)(1 - \exp(-c_l/L_p))] \tag{2}$$

In shape-persistent polymers, such as polyPPEs, the real chain can only bend at the atom positions, but not within the bonds, which behave as rigid segments. For such a segmented chain, deviations from the WLC model are expected, unless both the number n of segments in the chain and the number of segments within the persistence length, $n_p = L_p/l$, are large.

For polyPPEs, light-scattering experiments[49] and our own previous EPR results[31] indicate a persistence length of the order of 15 nm, corresponding to $n_p \approx 100$. Thus, significant deviations from the WLC model are expected only for short oligomers. However, due to the assumption of a fixed intersegment angle $\theta > 0$ the WLC model departs from the physical reality of a linear polymer, for which bond angles θ are distributed with maximum probability at $\theta = 0$. The shape of the distribution of θ is determined by the bending potential F and its width by the ratio between F and thermal energy kT. By abstracting from this distribution, the WLC model loses information on temperature dependence of the persistence length. This information has to be reintroduced *ad hoc*.[39]

To a good approximation, which is usually made in molecular force fields, the bending potential between two chemical bonds is a harmonic potential. This leads to a normal distribution of bond angles θ_j with variance

$$\langle \theta_j^2 \rangle = kT/2F_j \tag{3}$$

The HSC model is based on this approximation. In the basic form of the HSC model, we assume a uniform segment length l and a uniform bending potential F at all joints. The end-to-end-distance distribution $P(r_{EE})$ for $n = 50$ computed with the

(45) Cadiot. P.; Chodkiewicz, W. *Chemistry of Acetylenes*; Viehe, H. G., Ed.; Dekker: New York, 1969; pp 597−647.
(46) Further alternative synthetic strategies to oligoPPBs are opened through recently published work: Mössinger, D.; Jester, S.-S.; Sigmund, E.; Müller, U.; Höger, S. *Macromolecules* **2009**, *42*, 7974–7978. West, K.; Wang, C.; Batsanov, A. S.; Bryce, M. R. *Org. Biomol. Chem.* **2008**, *6*, 1934–1937.
(47) Kukula, H.; Veit, S.; Godt, A. *Eur. J. Org. Chem.* **1999**, 277–286.
(48) Porod, G. *Monatsh. Chem.* **1949**, *80*, 251–255.
(49) Cotts, P. M.; Swager, T. M.; Zhou, Q. *Macromolecules* **1996**, *29*, 7323–7328.

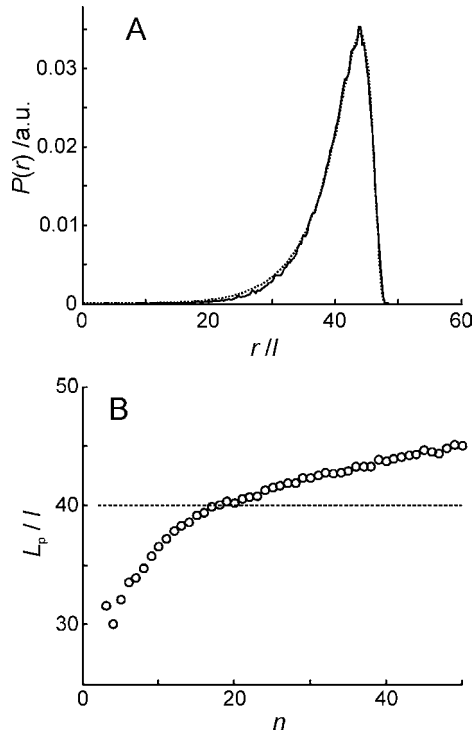

Figure 2. Comparison of the HSC and WLC model for shape-persistent polymers. (A) End-to-end distance distributions $P(r)$ as a function of the ratio between distance r and segment length l. The solid line is a simulation with the HSC model with bending potential $F/kT = 10$ and 50 segments, while the dotted line is a WLC model fit to this distribution. (B) Dependence of the normalized apparent persistence length L_p/l on the number of segments n in WLC model fits (circles) to end-to-end distance distributions obtained for HSC models with a bending potential $F/kT = 10$. The normalized contour length c_l/l equals n. The dashed line shows the estimate $4lF/kT$ of the persistence length for large segment numbers.

HSC model is shown in Figure 2A (solid line) together with its best fit by the WLC model with variable contour length c_l and L_p (dotted line), using the expressions of Wilhelm and Frey.[24] The fit reproduces the known contour length $c_l = nl$. The shape of the distribution is also almost perfectly reproduced. Similar quality of agreement is found for contour lengths up to the persistence length and slightly beyond that (data for other segment numbers not shown). However, the persistence length exhibits a dependence on contour length that is not expected within the WLC model (circles in Figure 2B). This dependence can be traced back to deviations of the approximate expressions for $P(r_{EE})$ within the WLC model[24] from the true distance distribution (Figure S1A, see Supporting Information).

The persistence length $L_{p,HSC}$ within the HSC model can be obtained by substituting $\langle\theta_j^2\rangle$ from eq 3 for θ^2 in eq 1,

$$L_{p,HSC} = 4lF/kT \qquad (4)$$

This estimate is indicated as a dotted line in Figure 2B. The number of segments within the persistence length is thus given by $4F/kT$. The mean square end-to-end distance for the HSC model can be derived by an approach due to Eyring[50] using eq 3. We find

$$\langle R^2\rangle_{HSC} = l^2\left[n + \sum_k^{n-1} 2(n-k)(1 - kT/4F)^k\right] \qquad (5)$$

By substituting the contour length $c_l = nl$ and the persistence length given by eq 4, the expression can be written with the same parameters as eq 2,

$$\langle R^2\rangle_{HSC} = (c_l/n)^2\left[n + \sum_k^{n-1} 2(n-k)(1 - c_l/nL_p)^k\right] \qquad (6)$$

For $F/kT = 25$, corresponding to 100 segments within the persistence length, deviations between the $\langle R^2\rangle$ predicted by eq 2 and 6 are less than 0.2% for $c_l < 1.5\ L_p$. These deviations are much smaller than the experimental error expected for the extraction of end-to-end distance distributions from DEER data. Thus, persistence lengths can be determined from $\langle R^2\rangle$ by numerically solving eq 2 for L_p. Compared to our previous approach[31] of fitting the distance distribution by approximate expressions for the WLC model,[14] the new approach avoids the problem of an apparent dependence of persistence length on contour length.

Results of DEER Experiments and Simulations

OligoPPE/Bs **Ia-d** (Chart 1) were available from our previous study.[31] The design of new series of model compounds was based on the following considerations. OligoPPEs **II** and **III** (Chart 1) consist of strictly alternating benzene and ethyne units and thus allow to exclude the influence of a butadiyne unit on flexibility. The use of two different spin labels, the conformationally flexible 1-oxyl-2,2,5,5-tetramethylpyrroline-3-carbonyloxy in oligoPPEs **II** and the conformationally unambiguous 1,1,3,3-tetramethyl-2-oxylisoindole-5,6-dicarboximide in oligoPPEs **III**, allows to test for stability of the separation of backbone and label contributions to the end-to-end distance distribution and to estimate the error in the backbone bending potential that arises from uncertainties in this separation. In particular, the conformationally unambiguous spin label[44,51] used in oligoPPEs **III** leads to a smaller label contribution to the width of the distance contribution and thus should allow for a more precise determination of the backbone bending potential. Finally, compounds **IV** are composed of strictly alternating benzene and butadiyne units. With the backbone bending potential for oligoPPEs already being known from analysis of series **II** and **III**, these compounds allow for determination of a separate bending potential for the link between two ethyne units.

Distance distributions were determined from primary DEER data of all compounds by background correction and subsequent Tikhonov regularization. As seen for the example of oligoPPEs **III** (Figure 3), these distributions exhibit the asymmetric shape expected for linear shape-persistent molecules with a contour length shorter than the persistence length[24] (compare Figure 2A). The width of the distributions increases significantly with increasing backbone length. This proves that our data contain information on backbone flexibility.

Preliminary data analysis was performed with the version of the HSC model used previously.[31] This model is moderately coarse-grained by substituting the benzene group by a single rigid segment. All other segments refer to bonds between two

(50) Eyring, H. *Phys. Rev.* **1932**, *39*, 746–748.

(51) Jeschke, G.; Sajid, M.; Schulte, M.; Godt, A. *Phys. Chem. Chem. Phys.* **2009**, *11*, 6580–6591.

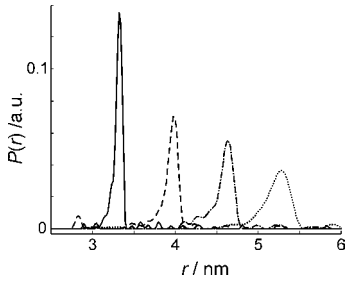

Figure 3. Experimental label-to-label distance distributions $P(r)$ obtained from DEER data by Tikhonov regularization for oligoPPEs **IIIa** (solid line), **IIIb** (dashed line), **IIIc** (dash−dot line), and **IIId** (dotted line).

atoms. In our previous work we assumed that the bending potential at the joint between the benzene group and the adjacent bond is only half as large as the other bending potentials. Now we tested how this assumption influenced the backbone end-to-end distance distributions extracted from the data. We found no significant dependence on the ratio of the bending potentials. Therefore, the model was simplified by assuming a uniform bending potential, except for the two joints in the center of the butadiyne unit that are encountered only in oligoPPE/Bs **I** and oligoPPBs **IV**. The standard deviation of segment lengths l_j was reexamined with longer 10 ns MD runs at 246 and 298 K, employing the pcff force field and an Andersen thermostat. The result suggests mean relative standard deviations $\sigma_l/l = 0.0132$ for a PPE unit and $\sigma_l/l = 0.0126$ for a PPB unit at the glass transition temperature of *o*-terphenyl, 246 K. We assumed a constant value of 0.013 and checked that minor variations did not influence the fits. The mean segment lengths of 0.2795 nm (benzene), 0.1430 nm (benzene−ethyne bond), 0.1201 nm (ethyne), and 0.1378 nm (ethyne−ethyne bond), originally taken from structures optimized with the MMFF94 force field,[52] were independently verified by DFT computations (see Supporting Information). The small deviations between the two sets of values are also insignificant.

This version of an HSC model with different segment lengths as well as an HSC model with uniform segment length l and the same mean relative standard deviations $\sigma_l/l = 0.013$ of bond lengths were tested against backbone end-to-end distance distributions retrieved from 10 ns long MD trajectories computed for a temperature of 298 K with the pcff force field (Figure 4). The WLC model was also included in this test. For the HSC model with uniform segment length l we assumed the mean segment length of a given backbone. Distributions for oligoPPE backbones with $n = 1, 2, 3, ...$ Six repeating units (see compound series **II** and **III** in Chart 1) were individually fitted by variation of two parameters. For HSC models these parameters were a uniform backbone bending potential F_g/kT and a backbone stretch factor s, while for the WLC model the free parameters were the persistence length L_p and contour length c_l. Variation of s and c_l slightly improved the fits and stabilized the values found for F_g/kT and L_p, although deviations of s from unity and c_l from the predicted contour length were generally less than 0.6%. Fit quality of the two HSC models is comparable and is slightly better than that obtained with the WLC model (Figures 4A and S2 [Supporting Information]).

The bending potentials F_g/kT obtained with HSC models (Figure 4B) with non-uniform (squares) and uniform (triangles) segment lengths differ slightly. With uniform segment length

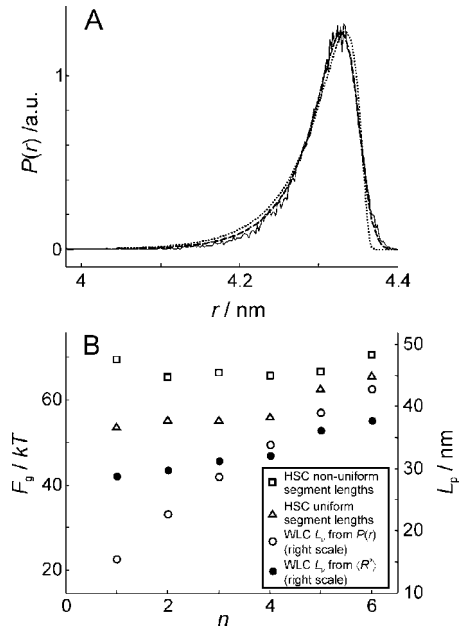

Figure 4. Fits of end-to-end distance distributions $P(r)$ extracted from 10 ns MD trajectories (pcff force field, 298 K) for oligoPPE backbones by HSC models and the WLC model. (A) $P(r)$ extracted from an MD trajectory for the unlabeled backbone of oligoPPE **IIe** (solid line), fit by the HSC model with non-uniform segment lengths (dashed line), and by the WLC model (dotted line). (B) Dependence of fit parameters on the number n of PPE units (see Chart 1). Squares and left vertical scale: bending potential F_g/kT in the HSC model with non-uniform segment lengths. Triangles and left vertical scale: bending potential F_g/kT in the HSC model with uniform segment lengths. Open circles and right vertical scale: Persistence length L_p in the WLC model determined by fitting the distance distributions by expressions from ref.[24] Full circles and right vertical scale: Persistence length L_p in the WLC model determined from $\langle R^2 \rangle$ by eq 2.

there appears to exist a slight trend in F_g/kT with chain length. With the more realistic non-uniform segment lengths no such trend is observed. The scatter of the data is due to statistical noise in the end-to-end distance distributions extracted from MD trajectories containing 20000 chain conformations. In contrast to the constant bending potential F_g/kT in the HSC model with non-uniform segment lengths, the persistence length L_p in the WLC model exhibits a clear trend with chain length (circles in Figure 4B). Note that the two vertical scales are related by eq 4, so that variations of F_g/kT and L_p can be directly compared in this plot.

In further test fits of individual experimental data series by the HSC model the stretch factor s assumed values slightly smaller or larger than unity for all sample series. Fixing this parameter to 1.0 did not lead to significant deterioration of fits and fixed values of s between 0.99 and 1.01 resulted in slightly different fit qualities, but not in significant changes of the other parameters. We thus eliminated the stretch factor s from the model to reduce the number of parameters.

The consolidated HSC model thus has five fixed parameters, the four segment lengths and a uniform relative standard deviation for them. In a global fit of the 16 experimental data sets (Figure 5) six further parameters are varied. These variable parameters are two backbone bending potentials F_g (general) and F_b (butadiyne unit), two label bending potentials F_f (conformationally flexible label employed in series **I**, **II**, and **IV**) and F_{cu} (conformationally unambiguous label employed in series **III**), and two label segment lengths l_f (conformationally flexible) and l_{cu} (conformationally unambiguous). When fitting

(52) Halgren, T. A. *J. Comput. Chem.* **1996**, *17*, 490–519.

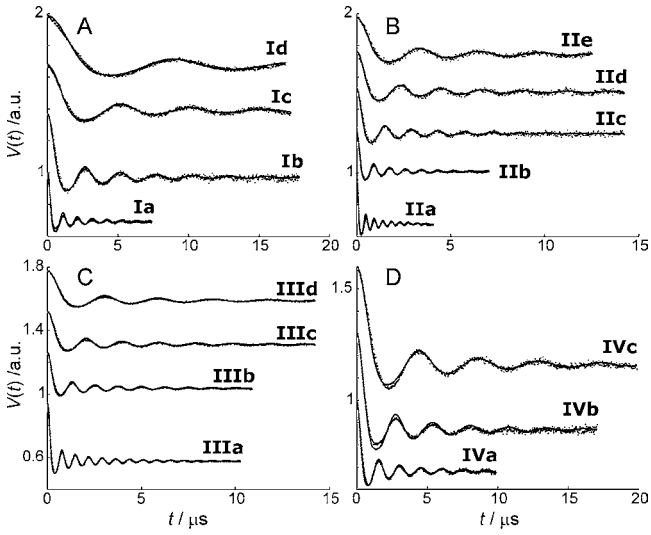

Figure 5. Global fit (solid lines) of background-corrected DEER time-domain data (dots) by the HSC model with non-uniform segment lengths (see bottom row and last column of Table 1). (A) oligoPPE/Bs **I**. (B) oligoPPEs **II**. (C) oligoPPEs **III**. (D) oligoPPBs **IV**.

data of only one series of compounds, only three (oligomers **II** and **III**) or four (oligomers **I** and **IV**) parameters are variable.

Fit residuals (Figure S3) indicate that systematic deviations are most prominent for the compounds with the shortest backbone, which is expected, as the segment model is a more serious approximation for the labels than for the backbone. The smallest systematic deviations are observed for the oligoPPEs **II** with flexible labels. This implies that the HSC model performs slightly worse for oligoPPE/Bs **I** and oligoPPBs **IV** with heterogeneous backbone bending potentials than for PPEs with homogeneous backbone bending potentials. The slightly larger residuals for oligoPPEs **III** (conformationally unambiguous labels) compared to oligoPPEs **II** (conformationally flexible labels) were originally unexpected. They are probably due to the anisotropy in bending of the conformationally unambiguous label (in-plane vs out-of-plane with respect to the conjugated system), which is not accounted for by the segment model. The systematic deviations even for the longer oligomers demonstrate that the HSC model does not perfectly describe backbone flexibility. Similar deviations are seen for the WLC model (data not shown). However these deviations do not change sign between different series of compounds and do not increase with backbone length. Hence, flexibility comparisons between different backbones as well as derivation of persistence lengths are meaningful.

As a first step in analyzing the data we performed fits of the background corrected time-domain data[31] for each individual series of oligomers with the consolidated HSC model (Figure S3). As seen in Table 1, highly consistent results for bending potentials are obtained from data series with the same type of label (oligomers **I**, **II**, **IV**). A somewhat smaller bending potential for the butadiyne unit compared to the uniform bending potential of phenyleneethynylene backbones is found for oligoPPE/Bs **I** and oligoPPBs **IV**. Together with the shorter average segment length in oligoPPBs compared to oligoPPEs this suggests a higher flexibility of oligoPPBs.

The uniform backbone bending potential F_g for oligoPPEs differs more strongly between series **II** and **III** with different labels and the same backbone than between series **I** and **II** with the same label and different backbones. This indicates some uncertainty in separation of the label and backbone contributions. However, a global fit of all data sets with the same bending potentials and label parameters does not lead to significant deterioration of fit quality for the individual series of data sets (compare last two columns of Table 1). Thus, all our data are consistent and the difference between bending potentials F_g obtained with the two different labels can be treated as a statistical error due to noise and deviations of the HSC model from experimental distance distributions.

To test the assumption of harmonic bending potentials we measured oligoPPE **IIIc** in solvents with different glass transition temperature T_g. This test is based on the assumption that, to first approximation, the conformational distribution of macromolecules is frozen at T_g, where characteristic times of system dynamics change by several orders of magnitude within a temperature range of a few Kelvin. Note that the true situation is somewhat more complex, as small regions may still rearrange below T_g.[53] As the end-to-end distance distribution is dominated by cooperative rearrangement of large parts of the backbone, corresponding to the slow modes in a normal-mode analysis, the smaller adjustments are assumed to be negligible within our experimental precision. In other words, structural changes that significantly influence the end-to-end distance distribution rely on the ability of the backbone to readjust its shape on the length scale of the end-to-end distance and this appears to be unlikely below T_g in a glassy matrix with a solvent molecule size that is much smaller than the end-to-end distance. Part of the remaining errors due to the assumption of freezing of all conformational changes at T_g are compensated by the fact that their influence also roughly scales with T_g and that this scaling is likely to be approximated by harmonic potentials, too.

The additional solvents used were 2-methyltetrahydrofuran deuterated in the methyl group (2-MTHF-d_3, $T_g = 91$ K), 1,2-di-*n*-butyl phthalate deuterated in the *n*-butyl groups (1,2-*n*-DBP-d_{18}, $T_g = 179$ K), and perdeuterated polystyrene (PS, $T_g = 373$ K). A factor of more than four between the lowest and highest glass transition temperature ensures that significant deviations from the behavior expected for a harmonic bending potential should be detected. The model compound was selected from series **III**, since the best fit quality is obtained with the conformationally unambiguous label. This makes the test of the assumption more strict than with conformationally flexible labels. Within series **III** the best compromise was sought between maximizing the influence of backbone flexibility by increasing backbone length and clearly observing the damping of the dipolar modulation during the maximum dipolar evolution time that could be achieved with all solvents.

The experimental data (dots in Figure 6) exhibit a significant dependence on T_g of the solvent that is most easily recognized by the shift of the local maximum near 2 μs toward shorter times for higher T_g. This shift corresponds to a decrease in the mean distance, as is expected when flexibility increases at higher temperature. Faster damping of the oscillations is also observed and corresponds to the expected broadening of the distance distribution at higher temperature. Both the decrease in mean end-to-end distance and the faster damping at a higher glass transition temperature were also observed for porphyrin-based molecular wires when comparing measurements in a toluene/pyridine mixture to measurements in perdeuterated *o*-terphenyl.[38]

(53) Debenedetti, P. G.; Stillinger, F. H. *Nature* **2001**, *410*, 259–267.

Table 1. Parameters of Least-Squares Fits of the HSC Model to Background Corrected DEER Time Domain Data[a]

data sets	F_g/kT	F_b/kT	F_f/kT	l_f/nm	F_{cu}/kT	l_{cu}/kT	rmsd[b]	rmsd[c]
Ia−d	25.0	20.2	7.74	0.640	−	−	0.00874	0.00883
IIa−e	25.2	−	7.33	0.633	−	−	0.00723	0.00732
IIIa−d	22.8	−	−	−	17.6	0.868	0.00391	0.00396
IVa−c	24.8	20.5	7.49	0.636	−	−	0.00815	0.00821
Global fit	24.2	20.8	7.33	0.638	17.8	0.867	−	0.00638

[a] Measured in perdeuterated *o*-terphenyl with a glass transition temperature of 246 K. F_g general backbone bending potential, F_b butadiyne unit bending potential, F_f conformationally flexible label bending potential, l_f conformationally flexible label length, F_{cu} conformationally unambiguous label bending potential, l_{cu} conformationally unambiguous label length, rmsd root-mean-square deviation, L_p apparent persistence length of the backbone. [b] Individual fits. [c] Global fit.

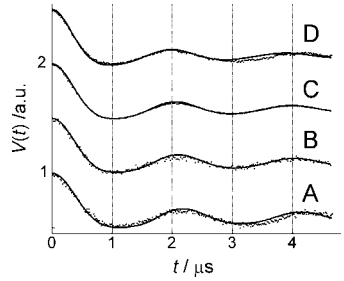

Figure 6. Dependence of backbone flexibility in oligoPPE **IIIc** on the glass transition temperature of the solvent. Background-corrected DEER time domain data (dots) are shown together with simulations by the HSC model (solid lines). The simulations are based on parameters determined on oligoPPEs **III** in perdeuterated *o*-terphenyl with glass transition temperature $T_g = 246$ K (see Table 1) and scaling of potential F_g/kT with the assumption $T = T_g$. No parameters were fitted. Dotted vertical lines are guides to the eyes. (A) Solvent 2-MTHF-d_3, $T_g = 91$ K. (B) Solvent 1,2-*n*-DBP-d_{18}, $T_g = 179$ K. (C) Solvent perdeuterated *o*-terphenyl, $T_g = 246$ K. (D) Solvent perdeuterated polystyrene, $T_g = 373$ K.

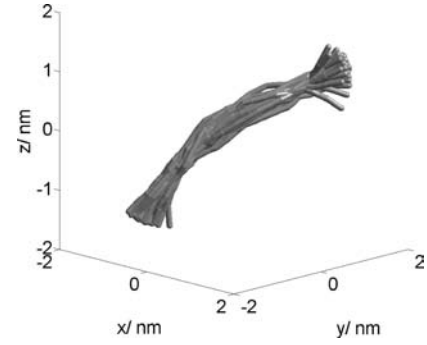

Figure 7. Visualization of the flexibility of the backbone of oligoPPE **IIe**. A superposition of 25 structures computed with the HSC model with $F_g/kT = 24.2$ is shown. The mean backbone vector is along the [1,1,1] direction.

The dependence of the data on T_g is well described by simulations that assume scaling of the normalized bending potential F_g/kT with $T = T_g$ (Figure 6, for residuals see Figure S6). Note that these simulations are based entirely on model parameters determined from the measurements of all compounds of series **III** in *o*-terphenyl. No further parameters are varied to reproduce the data obtained with the other solvents. In particular, the residual differences between simulation and experimental data for the other solvents are of similar magnitude and point to similar systematic deviations as for *o*-terphenyl, where the parameters were actually fitted. This implies that a normalized bending potential F_g/kT_g agrees with our data within the error introduced by the other simplifying assumptions. Except for 2-MTHF-d_3 as a solvent, data could also be obtained with a maximum dipolar evolution time of 9 μs. These data are also well reproduced by the simulations (Figure S7, Supporting Information).

Based on these results the ensemble of chain structures of oligoPPEs and oligoPPBs at ambient temperature can be computed at ambient temperature. Figure 7 shows a visualization of such an ensemble for the backbone of oligoPPE **IIe**.

Discussion

The end-to-end distance of a shape-persistent polymer chain depends on bending of its backbone. To characterize the flexibility of polymer backbones assembled from benzene and ethyne units, distance distributions between spin labels at the chain ends were measured by DEER spectroscopy for oligoPPEs, oligoPPBs, and oligoPPE/Bs. The shapes of these distributions at any given chain length can be fitted by an approximate expression for the WLC model, but the dependence of the shape and width on chain length is not in full agreement with these expressions (Figures 2, 4).

To quantify backbone bending from distance measurements between spin labels, the contribution of the labels to the distance distribution has to be separated from the contribution of the backbone. This requires models for the conformational distribution of both, the shape-persistent oligomer and the spin label. The model for the oligomer must provide, at least implicitly, not only the end-to-end distance distribution $P(r)$, but also the two-dimensional probability distribution $P_2(r, \chi)$ that correlates probabilities for a certain end-to-end distance r and a certain angle χ between the direction vectors at the chain ends.

Monte Carlo computations of the HSC model provide $P_2(r, \chi)$. In this model the chain consists of rigid segments with normally distributed intersegment angles θ_j with mean values $\langle\theta_j\rangle = 0$ and uniformly distributed torsion angles ϕ_j. This corresponds to a harmonic bending potential at the joints between segments and free rotation. For oligoPPEs and related compounds the rigid segments are identified with bonds, except for the benzene ring which is modeled as a single segment. This coarse graining of the benzene ring is necessary to preserve the linear topology of the chain.

Compared to the WLC model, which implicitly assumes fixed nonzero intersegment angles, the HSC model provides a more realistic description of molecular mechanics of linear, shape-persistent polymer chains. This is apparent in slightly better fits of end-to-end distance distributions extracted from atomistic MD simulations. More significantly, when varying the chain length in the MD simulations a constant bending potential is found for the HSC model while an unexpected trend in the persistence length is observed for the WLC model (Figure 4).

Unlike the basic WLC model the HSC model can predict changes in the end-to-end distance distribution with temperature, eq 2. With the further assumption that the ensemble of chain conformations observed in frozen glassy solutions at a temperature of 50 K is determined by the glass transition temperature T_g of the solvent, the dependence of DEER data on T_g can be

predicted. Indeed, such a dependence is observed and is well described by the prediction of the HSC model (Figures 6, S4). The HSC model is thus in full agreement with experimental observations for the shape-persistent oligomers studied in this work.

Thus, flexibility of polyPPEs and polyPPBs is best described by harmonic bending potentials within the HSC model. Considering the variation between experimentally determined bending potentials for different series of oligomers (Table 1), we arrive at a uniform bending potential $F_g/kT = 24.2 \pm 2.0$ for joints in the HSC model of polyPPEs and a slighly smaller bending potential $F_g/kT = 20.8 \pm 2.0$ for joints between two ethyne units in polyPPBs. These values correspond to the glass transition temperature of *o*-terphenyl $T_g = 246$ K. Expressed as molar bending energies per joint, the values are (49.5 ± 4.1) kJ mol^{-1} and (42.5 ± 4.1) kJ mol^{-1}.

Similar to the fits of MD-derived end-to-end distance distributions by approximate formulas for the WLC model (Figure 4), fits of the experimental end-to-end distance distributions extracted by the HSC model by the WLC model result in an unexpected trend of the apparent persistence length L_p (data not shown). In contrast, analysis of the mean square end-to-end distance $\langle R^2 \rangle$ by eq 2 provides values whose variation with chain length is less than their error estimated from the uncertainty in the bending potentials (Figure S8). We thus obtain persistence lengths at 246 K of (16.7 ± 1.5) nm for polyPPE and of (14.3 ± 1.5) nm for polyPPB. Despite the overlap of the error bars, the slightly larger flexibility of polyPPB compared to polyPPE is an established fact, since it is directly seen when comparing data of oligoPPEs **II** and oligoPPBs **IV**. According to eq 4 these values correspond to persistence lengths at 298 K of (13.8 ± 1.5) nm for polyPPE and (11.8 ± 1.5) nm for polyPPB.

Compared to atomistic MD simulations the HSC model achieves a significant reduction in the number of parameters and a significant reduction in the computational effort for computing end-to-end distance distributions $P(r)$ and two-dimensional probability distributions $P_2(r, \chi)$. These two-dimensional distributions correlate the probability to observe a certain end-to-end distance r with the probability to observe a certain angle χ between the direction vectors at the chain ends. Differences in $P(r)$ between MD simulations and the HSC model are small (Figure 4A), as are differences in $P_2(r, \chi)$ (Figure S9). As already found in our previous work[31] the flexibility predicted by molecular force fields deviates strongly from the one found by fits of experimental distance distributions (compare F_g/kT in Figure 4 and Table 1). A deviation is expected, as force fields are parametrized on a limited set of low-molecular weight compounds and errors in bending potentials become more serious for extrapolation to polymer chains. As already pointed out in work on flexibility of bis-peptides,[36] improvement of a molecular force field on the basis of EPR data for end-to-end distance distributions is not feasible, as the number of variable force field parameters is too large compared to the information content of the experimental data. Indeed, the success of the HSC model in describing our data and data extracted from MD trajectories proves that the number of parameters can be significantly reduced if only the conformational distribution of the polymer backbone is of interest.

Conclusion

The flexibility of shape-persistent oligomers can be quantitatively characterized by DEER distance distribution measurements between spin labels attached to their chain ends. Such experimental data are well described by the newly introduced HSC model, even for short chain lengths. In the HSC model for polyPPEs, flexibility is quantified by a uniform harmonic bending potential. Two separate bending potentials are assumed for polyPPBs, which are found to have a slightly higher flexibility. Variation of the spin label structure allows for an estimate of the error in the separation of spin label and backbone contributions to the distance distribution. This error causes an uncertainty of about 10% in the harmonic bending potential. The HSC model can predict temperature dependence of flexibility. This was tested by varying the glass transition temperature of the solvent between 91 and 373 K and the prediction was found to be consistent with experimental data. Our data suggest persistence lengths at 298 K of (13.8 ± 1.5) nm for polyPPE and of (11.8 ± 1.5) nm for polyPPB.

Experimental Methods

Syntheses of Spin-Labeled Oligomers. The syntheses of spin-labeled oligoPPE/Bs **I**[31,54] and spin-labeled oligoPPEs **IIa**[54] and **IIIa**[44] have been described. The syntheses of the other spin-labeled oligomers and all other experimental methods are given in detail in the Supporting Information.

Acknowledgment. We thank René Tschaggelar and Enrica Bordignon for implementing the second frequency source on the pulse EPR spectrometer. Financial support by DFG projects JE 246/4-2 and GO 555/4-3 is gratefully acknowledged.

Supporting Information Available: Computational procedure for a DFT computation of segment lengths, DFT derived segment lengths, fit of an MD derived end-to-end distance distribution by the HSC model with uniform segment length, fit residuals for the HSC model, HSC model fits of individual series of data sets, experimental distance distributions for all compounds, fit residuals for dependence on solvent T_g, dependence on solvent T_g with a dipolar evolution time of 9 μs for three solvents, comparison of two-dimensional probability distributions $P_2(r, \chi)$ derived from an MD run and by the HSC model, experimental procedures including analytical data of all newly synthesized compounds, and ^{1}H NMR data of spin-labeled oligomers and some synthetic intermediates. This material is available free of charge via the Internet at http://pubs.acs.org.

JA102983B

(54) Godt, A.; Franzen, C.; Veit, S.; Enkelmann, V.; Pannier, M.; Jeschke, G. *J. Org. Chem.* **2000**, *65*, 7575–7582.